POLYPUBLIE

Improving fatigue evaluations of structures using in-service behavior measurement data

Romain Pasquier, James Alexandre Goulet, Claire Acevedo, Ian F. C. Smith

Document en libre accès dans PolyPublie
Open Access document in PolyPublie

Date	2014
Type	Article de revue / Article
Version	Version finale avant publication / Accepted version
URL de PolyPublie PolyPublie URL	https://publications.polymtl.ca/2893/
Évaluation par les pairs Peer reviewed	Révisé par les pairs / Refereed
Conditions d'utilisation Terms of use	© Tous droits réservés / All rights reserved
Référence Citation	Pasquier, R., Goulet, J. A., Acevedo, C., & Smith, I. F. C. (2014). Improving fatigue evaluations of structures using in-service behavior measurement data. Journal of Bridge Engineering, 19(11), 1-10. https://doi.org/10.1061/%28asce%29be.1943-5592.0000619

Publication officielle
Official publication

Titre de la revue Journal title	Journal of Bridge Engineering (vol. 19, no. 11)
Maison d'édition Publisher	ASCE
URL officielle Official URL	https://doi.org/10.1061/%28asce%29be.1943-5592.0000619
Mention légale Legal notice	This material may be downloaded for personal use only. Any other use requires prior permission of the American Society of Civil Engineers. This material may be found at https://doi.org/10.1061/%28asce%29be.1943-5592.0000619

Ce fichier a été téléchargé à partir de PolyPublie, le dépôt institutionnel de Polytechnique Montréal
This file has been downloaded from PolyPublie, the institutional repository of Polytechnique Montréal
https://publications.polymtl.ca

POLYPUBLIE
Polytechnique Montréal

POLYTECHNIQUE MONTRÉAL
LE GÉNIE EN PREMIÈRE CLASSE

Titre: Title:	Improving fatigue evaluations of structures using in-service behavior measurement data
Auteurs: Authors:	Romain Pasquier, James-A. Goulet, Claire Acevedo et Ian F.C. Smith
Date:	2014
Type:	Article de revue / Journal article
Référence: Citation:	Pasquier, R., Goulet, J.-A., Acevedo, C. & Smith, I. F. C. (2014). Improving fatigue evaluations of structures using in-service behavior measurement data. *Journal of Bridge Engineering*, *19*(11), p. 1-10. doi:10.1061/(asce)be.1943-5592.0000619

Document en libre accès dans PolyPublie
Open Access document in PolyPublie

URL de PolyPublie: PolyPublie URL:	https://publications.polymtl.ca/2893/
Version:	Version finale avant publication / Accepted version Révisé par les pairs / Refereed
Conditions d'utilisation: Terms of Use:	Tous droits réservés / All rights reserved

Document publié chez l'éditeur officiel
Document issued by the official publisher

Titre de la revue: Journal Title:	Journal of Bridge Engineering
Maison d'édition: Publisher:	ASCE
URL officiel: Official URL:	https://doi.org/10.1061/(asce)be.1943-5592.0000619
Mention légale: Legal notice:	"Authors may post the final draft of their work on open, unrestricted Internet sites or deposit it in an institutional repository when the draft contains a link to the bibliographic record of the published version in the ASCE Library or Civil Engineering Database"

Ce fichier a été téléchargé à partir de PolyPublie, le dépôt institutionnel de Polytechnique Montréal
This file has been downloaded from PolyPublie, the institutional repository of Polytechnique Montréal

http://publications.polymtl.ca

R. Pasquier, J.-A. Goulet, C. Acevedo and I. F.C. Smith, (2014).
Improving Fatigue Evaluations of Structures Using In-service Behavior Measurement Data.
Journal of Bridge Engineering, 19(11), 04014045. doi:10.1061/(ASCE)BE.1943-5592.0000619

Improving Fatigue Evaluations of Structures Using In-service Behavior Measurement Data

Romain Pasquier[1]; James-A. Goulet, A. M. ASCE [2];

Claire Acevedo[3]; and Ian F. C. Smith, F. ASCE[4]

Abstract

Conservative models and code practices are usually employed for fatigue-damage predictions of existing structures. Direct in-service behavior measurements are able to provide more accurate estimations of remaining-fatigue-life predictions. However, these estimations are often accurate only for measured locations and measured load conditions. Behavior models are necessary for exploiting information given by measurements and predicting the fatigue damage at all critical locations and for other load cases. Model-prediction accuracy can be improved using system identification techniques where the properties of structures are inferred using behavior measurements. Building upon recent developments in system identification where both model and measurement uncertainties are considered, this paper presents a new data-interpretation framework for reducing uncertainties related to prediction of fatigue life. An initial experimental investigation confirms that, compared to traditional engineering approaches, the methodology provides a safe and *more realistic* estimation of the fatigue reserve capacity. A second application on a full-scale bridge also confirms that using load-test data reduces the uncertainty related to remaining-fatigue-life predictions.

Keywords: Remaining fatigue life; Model-based data interpretation; Population of models; Uncertainty; Conservatism.

[1]Applied Computing and Mechanics Laboratory (IMAC), School of Architecture, Civil and Environmental Engineering (ENAC), École Polytechnique Fédérale de Lausanne (EPFL), CH-1015 Lausanne, Switzerland

[2]Department of Civil and Environmental Engineering, University of California, Berkeley,USA

[3]Ritchie Group, Materials Sciences Division, Lawrence Berkeley National Laboratory, Berkeley, and Department of Materials Science and Engineering, University of California, Berkeley,USA

[4]Applied Computing and Mechanics Laboratory (IMAC), School of Architecture, Civil and Environmental Engineering (ENAC), École Polytechnique Fédérale de Lausanne (EPFL), CH-1015 Lausanne, Switzerland

R. Pasquier, J.-A. Goulet, C. Acevedo and I. F.C. Smith, (2014).
Improving Fatigue Evaluations of Structures Using In-service Behavior Measurement Data.
Journal of Bridge Engineering, 19(11), 04014045. doi:10.1061/(ASCE)BE.1943-5592.0000619

INTRODUCTION

The evaluation of existing structures is often based on conservative models and code practices. When such provisions require strengthening or replacement, alternative actions may take advantage of behavior measurements (e.g. displacements, tilts, strains and accelerations) for reducing model-prediction uncertainties. Measured data is often able to improve evaluation of the in-service behavior of structures, thereby avoiding costly interventions and sometimes, structural replacement. During the last decade, cheap and reliable measuring instruments have been commercialized, simplifying the measurement of structures. For existing bridges, many methodologies are available to perform fatigue assessment using stress-range measurements of critical details. Some of them use measurement data for predicting remaining fatigue life at monitored locations using various fatigue models (Sweeney 1976; Chan et al. 2001; Ye et al. 2012; Zhou 2006; Soliman et al. 2013). Others evaluate the fatigue reliability of monitored bridge details (Guo and Chen 2013; Orcesi and Frangopol 2010). However, even if the fatigue assessment is accurate at the measured locations, the information obtained from measurements cannot be extrapolated to predict the fatigue damage at other locations without using behavior models (Papadimitriou et al. 2011). In addition, the number of measurement locations is generally limited by practical considerations. Furthermore, the measurements fall short of providing information related to conditions other than those prevailing during monitoring (e.g. for other load configurations).

Behavior models of structures are needed for evaluating stress ranges at locations where measurements are not available. Several studies have validated and calibrated behavior models by comparing analytical results with field measurements in order to make fatigue assessments at other critical locations of the structure (Siriwardane et al. 2008; Liu et al. 2010; Guo et al. 2012; Uzgider et al. 1996). Generally, such assessments do not explicitly account for model and measurement uncertainties. Simple comparisons of model predictions with measurements are often not sufficient to ensure the accuracy of model predictions. Model-based data-interpretation techniques (including model and measurement uncertainties) link structural response to structural properties, thereby improving remaining-fatigue-life estimations (prognosis). Several techniques exist for data inter-

pretation; three common families of approaches are model calibration, Bayesian inference and model falsification.

Researchers have already identified that only in specific circumstances, predictions can be improved by model calibration (Beven 2006; Beven et al. 2008). This is because calibration implies, among other factors, that errors occurring during prognosis are the same as errors occurring during calibration. Therefore, the validity of the prognosis is often limited to the domain of the calibration data (ASME 2006). In practical applications, models are required to be able to perform predictions for quantities that are not measured due to a range of technological, economic and practical reasons.

Other probabilistic data-interpretation techniques such as Bayesian inference (MacKay 2003; Yuen 2010) are available for improving the knowledge of model parameters and for comparing several model classes. Many examples have been reported where Bayesian methodologies lead to correct diagnoses and prognoses in situations where information is available for defining the joint probability density function (PDF) of error (Strauss et al. 2008; Cheung and Beck 2009; Zhang et al. 2011). However, the literature has a poor record of presenting full-scale civil-engineering examples where it is common to have systematic bias in model predictions due to omissions and simplifications in behavior models. Goulet et al. (2012) proposed a population-based model falsification technique for system identification. This methodology is most appropriate for performing diagnosis when the probability density function of errors is poorly defined (Goulet and Smith 2013a).

This paper presents a new data-interpretation framework for reducing uncertainties related to the prediction of fatigue life. This framework extends the model-falsification diagnosis methodology for performing more accurate prognoses. Here, prognoses are probability density functions describing the remaining fatigue life of structures. The first section of this paper presents the prognosis methodology and the second section presents two large-scale case studies where static measurements are used for reducing the prediction uncertainty.

POPULATION-BASED PROGNOSIS METHODOLOGY

The methodology proposed in this paper consists of the following steps: (1) create a population of model instances representing a structure, (2) perform behavior measurements such as displacement, tilts, strains and accelerations, (3) falsify inadequate model instances by comparing their predictions with the measured responses, and (4) perform prognosis using the population of models that have not been falsified. The falsification of models in step (3) usually leads to a reduction of the prediction uncertainty. The data-interpretation methodology that is used to determine whether or not model instances are compatible with observations is described in the next subsection. A second subsection presents the remaining-fatigue-life prognosis methodology based on model populations.

Model falsification

Model falsification was proposed as a model-based data-interpretation methodology for situations where little information is available for describing the PDF of prediction errors (Goulet and Smith 2013b; Goulet et al. 2012). In order to represent the behavior of a bridge, a model is created among several possible classes of models. This model is usually based on the finite-element method and takes as input a set of n_p physical parameters, $\boldsymbol{\theta} = [\theta_1, \theta_2, ..., \theta_{n_p}]$ describing the unknown geometrical, physical and material characteristics of the structure. Model falsification is based on the comparison of the predicted ($\mathbf{g}_i(\boldsymbol{\theta})$) and measured ($y_i$) such that:

$$\mathbf{g}_i(\boldsymbol{\theta}) - y_i = \epsilon_{model,i} - \epsilon_{measure,i} \tag{1}$$

where $\epsilon_{model,i}$ and $\epsilon_{measure,i}$ are the model and measurement errors; and i refers to the location where these values are compared. The *observed residual* is defined as the difference between the predicted values and observed values. Errors originating from both the model and measurements, are treated as random variables $U_{model,i}$ and $U_{measure,i}$. Some sources of model uncertainties can be explicitly quantified (e.g., the geometric variability of the structure, the variability of material properties and mesh-refinement uncertainty of the finite-element model). In most cases, other sources such as model-simplification uncertainties are defined using engineering heuristics.

Measurement uncertainties are due to sensor resolution, cable losses and measurement repeatability. These sources of uncertainty are estimated based on manufacturer specifications or domain heuristics. All of these uncertainties are represented by a single random variable $U_{c,i}$ representing possible outcomes $\epsilon_{c,i}$ of the differences between predicted and measured values. An instance of $\boldsymbol{\theta}$ is falsified if, for any measurement location, the difference between predicted and measured values is outside the interval defined by threshold bounds such that the expression displayed in Equation 2 is not satisfied.

$$\forall i \in \{1, \ldots, n_m\} : \; T_{low,i} \leq \mathbf{g}_i(\boldsymbol{\theta}) - y_i \leq T_{high,i} \tag{2}$$

Conversely, a model instance is accepted only if this difference lies inside the bounds at every location.

Threshold bounds are determined specifically for every location based on the PDF describing the combination of all uncertainty sources. Threshold bounds are defined as the shortest intervals which simultaneously include a target probability and satisfy

$$\phi^{1/n_m} = \int_{T_{low,i}}^{T_{high,i}} f_{U_{c,i}}(\epsilon_{c,i}) d\epsilon_{c,i} \quad \forall i \in \{1, \ldots, n_m\} \tag{3}$$

where ϕ corresponds to the target probability that the right model will not be falsely discarded. This way of defining threshold bounds (Eq. 3) uses the Šidák correction employed for statistical tests when the variance is known and the dependencies are unknown (Šidák 1967). This method has the advantage of providing conservative threshold bounds, regardless of the dependencies between uncertainties (JCGM 2011).

All model instances that are not falsified remain in the candidate model set, which is a subset that is composed of the identified parameter values $\boldsymbol{\theta}^* = [\theta_1^*, \theta_2^*, ..., \theta_{n_p}^*]$. This subset contains model instances that are compatible with measurements given the model and measurement uncertainties. The measurements that are used during data interpretation should be at those locations identified as the most sensitive to the unknown parameters. Using measurements at locations that are not sensitive to the parameters is not an efficient approach. Despite this, as long as uncertainties

are conservatively estimated, including more measurements cannot bias the selection of candidate models.

Moreover, the choice of the model parameterization (model class) is a challenge for any data-interpretation approach. Currently, the only solution is to rely on engineering heuristics and experience. Despite this, the model-falsification approach offers an advantage compared with traditional approaches; it is possible to falsify the entire model class when the parameterization is inadequate. Goulet and Smith (2013a) provide examples of how model-class falsification can identify wrong model parameterizations.

Traditional model updating, in most cases, identifies models that minimize the difference between predicted and measured values. This procedure has limited potential for predicting values at locations other than those measured. With model falsification, a model instance which is falsified by a set of measurements is an incorrect model and thus, is not capable of correctly predicting the values at any location. This is the benefit of using model falsification for fatigue prognosis. Therefore, rather than searching for so-called optimal model instances for predicting the values, the model-falsification approach identifies model instances which can be omitted. This different perspective leads to better predictions at locations that are not measured.

Population-based fatigue prognosis

Recent advances in computing power allow interpretation of data and calculation of predictions for populations of models. Instead of performing predictions on a unique model class and on a unique set of parameter values, all candidate models that are identified are employed to yield a distribution of predicted values. For fatigue predictions, a number of cycles under constant stress-range level are generally used during the design of critical construction details. For the evaluation of remaining fatigue life, other approaches compute stress history using traffic-loading simulations. These approaches usually lead to more accurate predictions, at the expense of being more demanding on computing resources. The approach that is presented in typical construction codes (AASHTO 2007; EN1993-1-9 2005; SIA263 Code 2003) uses a single traffic-axle loading and constant stress amplitudes for determining the remaining number of cycles to failure. This

simplified approach has been used for evaluating the number of cycles to failure because it requires a small amount of computing resources and it returns conservative remaining-life predictions.

For a bridge, the constant stress-amplitude calculations are performed by calculating the influence line resulting from a traffic-axle loading applied on a finite-element model. Maximum and minimum stresses are extracted from the influence line. The difference between these values is

$$\Delta\sigma = \sigma_{max} - \sigma_{min} = S_n \tag{4}$$

where S_n is the maximum stress range inducing damage to a critical construction detail (Fisher et al. 1998). This stress range is determined for each critical construction detail and for each candidate finite-element model. The number of cycles to failure is then determined for each stress range through S_n-N_f curves which are obtained from empirical investigations and are available in construction codes and design guides (SIA263 Code 2003; Zhao et al. 2002). These curves represent the number of stress-range cycles that are needed to reach the failure of a construction detail. The relation between the stress range S_n and the number of cycles to failure N_f is

$$N_f = C \cdot S_n^{-m} \tag{5}$$

where C is a constant depending on the detail category and m is a measure of the fatigue crack-grow rate. The constants C and m are determined experimentally. Equation 5 provides the number of cycles for a single model instance. For population-based prognosis, both variabilities due to parameters $\boldsymbol{\theta}$ and due to model uncertainties have to be included in the remaining-fatigue-life predictions. Thus, the distribution of the candidate-model stress-range values is combined with the distribution of the model prediction error for each of the n_{cd} critical details. The calculation of the number of cycles determined for an instance of candidate-model stress range and model error for the critical detail j is described by

$$\forall j \in \{1, \ldots, n_{cd}\} : N_{f,j} = C \cdot \Delta\sigma_j^{-m} = C \cdot (\Delta\mathbf{g}_j(\boldsymbol{\theta}^*) - \Delta\epsilon_{model,j})^{-m} \tag{6}$$

where $\Delta g_j(\boldsymbol{\theta}^*)$ is the stress-range value obtained for one instance of the candidate model set and $\Delta\epsilon_{model,j}$ is a sample of the model stress-range uncertainty. Model stress-range uncertainty originates from the same sources described in the previous section and is evaluated for the critical locations studied, except for the geometric variabilities which are already included in the constant C. Values for the constant C already include uncertainty due to detail geometry since the empirical determination of C involves a database of test results and calculation of a 95% confidence level (Hobbacher 2012). For each critical detail, this procedure leads to a PDF describing the number of cycles to failure. The number of cycles are then transformed to time units according to the frequency of the transit of heavy-vehicles on the bridge.

Figure 1 presents a flowchart summarizing each step of the prognosis methodology that was described in this section. In this flowchart, the result of the remaining-fatigue-life prediction is shown for a single critical construction detail. This methodology should be repeated for each detail critical to the structural safety.

CASE STUDIES

This section presents two applications of the population-based prognosis methodology. The first case study involves a truss beam that was tested under cyclic loading. The second application is the Aarwangen Bridge (Switzerland) where strains were measured during static-load tests. For both applications, the prognosis approach presented in this paper is compared with a conservative engineering approach. For the truss-beam example, the prognosis approach is also compared with fatigue-failure observations obtained experimentally.

Truss-beam example

Truss-beam and test description

This first case study investigates the fatigue resistance of a steel tubular truss beam that was designed, fabricated and welded to mimic real truss-bridge constructions. In order to obtain a similar fatigue behavior to full-scale bridges, the size of the beam is chosen to be similar to the size of conventional tubular-truss bridge beams (i.e. $8.6\,\text{m}$ long and $1.8\,\text{m}$ high). The specimen is composed of Circular Hollow Section (CHS) members; two brace branches are welded onto

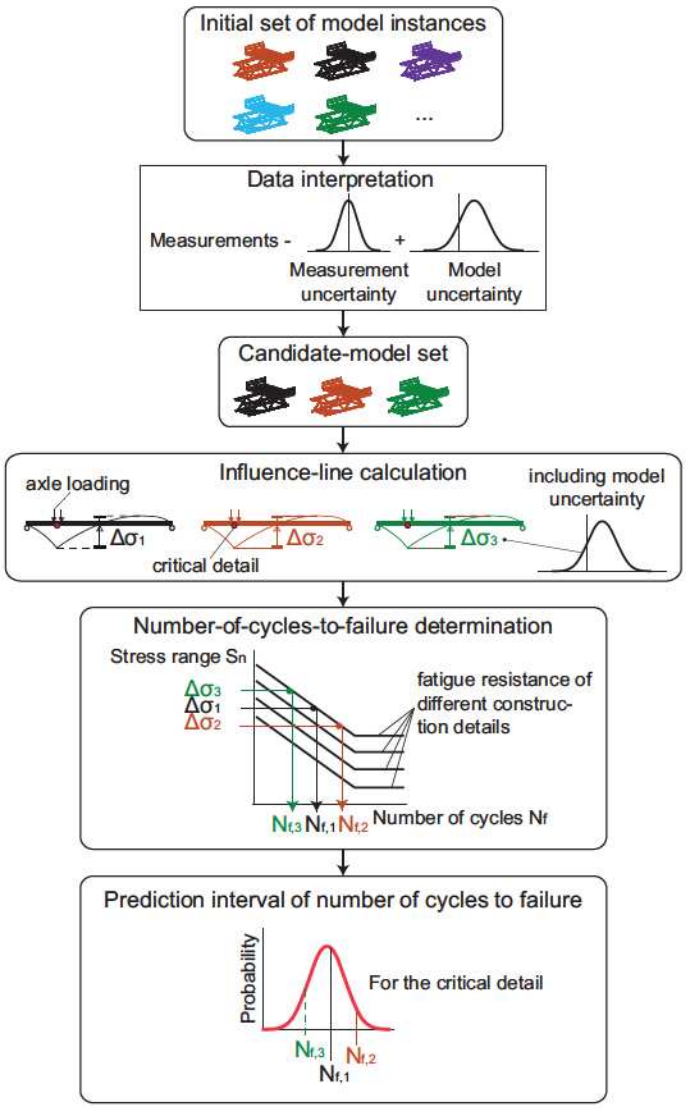

Figure 1. Methodology flowchart

continuous chords in order to form K-joints. Figure 2 shows the dimensions and configuration of the truss-beam along with the position of uniaxial strain gauges and displacement transducers. Both ends of the upper chord are simply-supported by steel plates; the upper chord is clamped with straps on its supports to prevent any uplift during testing. The supporting plates are 150 mm wide and their edges are positioned at 40 mm from the brace-to-chord weld heel.

This planar truss beam was tested with static and cyclic loading in order to study the behavior of four K-joints (joints #3N, #1, #2 and #3S). Joints at support and actuator locations have been

R. Pasquier, J.-A. Goulet, C. Acevedo and I. F.C. Smith, (2014).
Improving Fatigue Evaluations of Structures Using In-service Behavior Measurement Data.
Journal of Bridge Engineering, 19(11), 04014045. doi:10.1061/(ASCE)BE.1943-5592.0000619

treated to prevent cracking. A cyclic concentrated load is applied at mid-span on the upper chord with a load cycle amplitude of 550 kN.

Strain-gauge measurements obtained during the initial static test are used to identify the model instances that are compatible with structural observations. Experimental strain data indicate that there is a difference of up to 13% for strain gauges that are symmetrically positioned with respect to the structure and the load (gauges #35-#37 versus gauges #43-#45). This phenomena is explained by asymmetrical boundary conditions caused by the straps used to secure the experimental set-up. The rotational constraint due to the boundary condition is modeled using a rotational spring, for which the stiffness parameter needs to be identified. Because the real position and stiffness of the straps on both ends of the beam are unknown, both the southern and northern supports have independent parameter values. For the same reason, two additional parameters describe the uncertain southern and northern support drift from the middle of the support plate. In addition, the Young's modulus of the steel truss and the rotational stiffness of the welded connections are parametrized. The six unknown parameters $\boldsymbol{\theta}$ and their initial values are presented in Table 1. Figure 3 presents six axes describing each parameter value. The full dots are the falsified parameter values and the squares represent the identified parameter values. This figure also presents an example of model instance defined by the combination of a specific value for each physical parameter. The initial model set contains $24\,500$ model instances. Figure 4 describes the finite-element model and the parameters that are used for data interpretation.

Table 1. Truss-beam parameter ranges, the number of divisions and the identified range of parameter values

Parameter θ	Units	Initial range	Number of divisions	Identified range
Young's modulus of steel	GPa	207-210	4	207-209
Rotational stiffness of truss connections	MNm/rad	10^{-1}-10^{3}	5	10-10^{3}
Rotational stiffness of the southern support	MNm/rad	10^{-1}-10^{3}	5	10^{-1}-10
Rotational stiffness of the northern support	MNm/rad	10^{-1}-10^{3}	5	10
Southern support drift	mm	0-150	7	0-150
Northern support drift	mm	0-150	7	75

R. Pasquier, J.-A. Goulet, C. Acevedo and I. F.C. Smith, (2014).
Improving Fatigue Evaluations of Structures Using In-service Behavior Measurement Data.
Journal of Bridge Engineering, 19(11), 04014045. doi:10.1061/(ASCE)BE.1943-5592.0000619

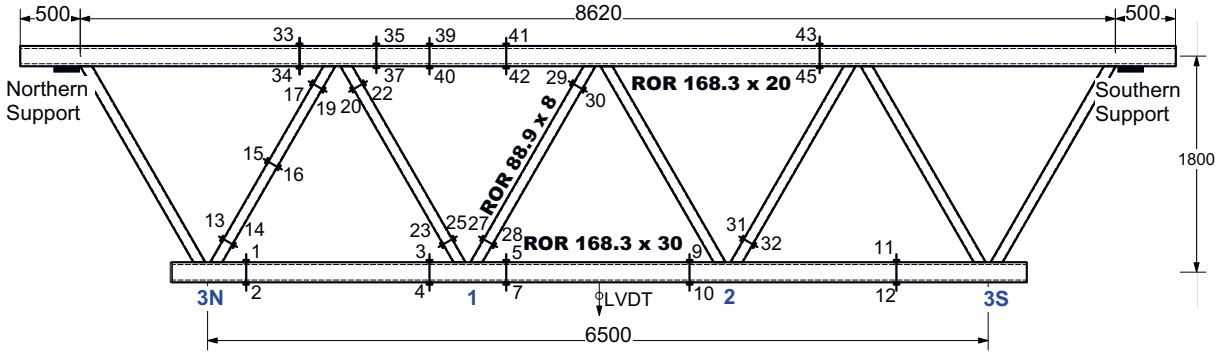

▪ Uniaxial strain gauges (46): HBM 1-LY11-10/120

Figure 2. Positions of uni-axial strain gauges and linear variable displacement transducer (LVDT) on the truss beam (numbers refer to strain-gauge labels)

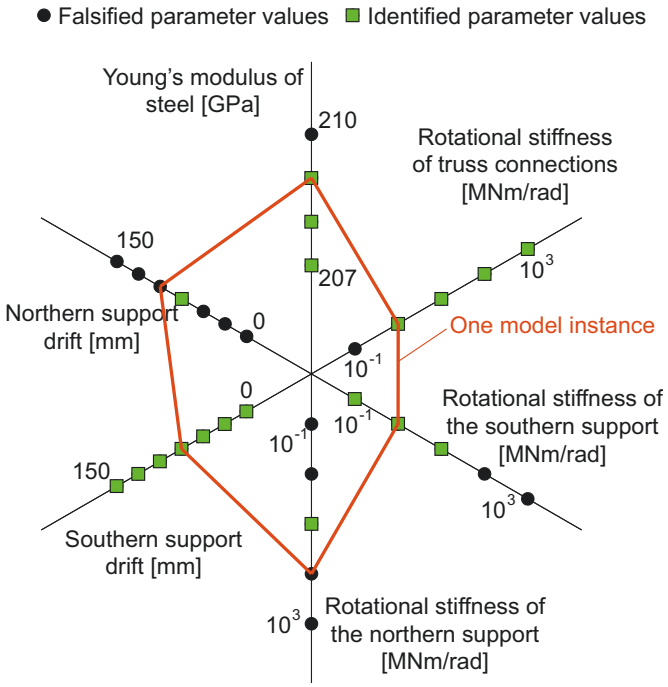

Figure 3. An example of model instance with falsified and identified parameter values for the truss beam

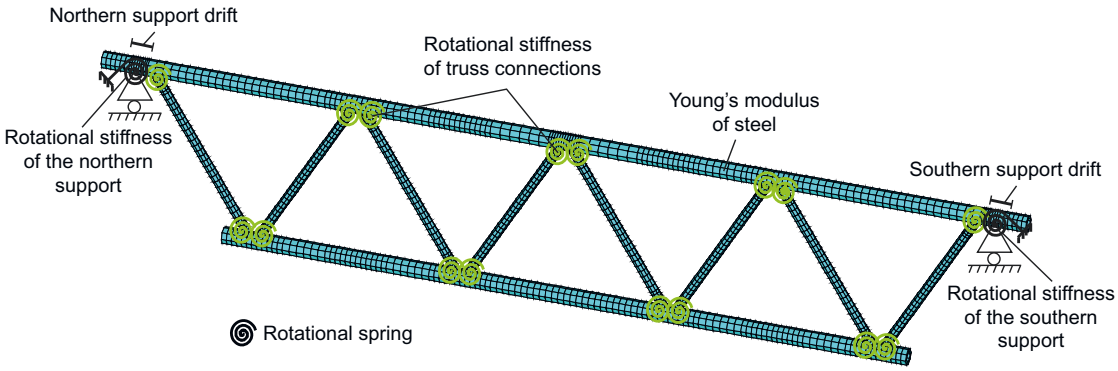

Figure 4. Finite-element model of the tubular truss beam and parameter description

Uncertainty sources for $U_{model,i}$ and $U_{measure,i}$ are presented in Table 2 along with their probability density function. Profile dimension variabilities are based on tolerance values that are available in the steel construction table (SZS 2005) with respect to the design values. Their uncertainty is estimated through evaluation of model-prediction variance using Monte Carlo sampling. Other uncertainties are estimated using field data and engineering heuristics. Model simplifications and FEM uncertainties are evaluated with respect to the mean of the initial-model-set prediction values.

Table 2. Truss-beam uncertainty sources and their estimated probability density function

Uncertainty source	Units	PDF	Min	Max	With respect to
Profile thickness variability	%	Uniform	-12.5	12.5	design thickness value
Profile diameter variability	%	Uniform	-1	1	design diameter value
Sensor resolution	μmm/mm	Uniform	-2	2	-
Cable losses	%	Uniform	-0.25	0.25	measurement value
Model simplifications and FEM	%	Uniform	0	5	mean prediction value

From $24\,500$ initial model instances, only 107 are compatible with the 34 strain measurements. When including model and measurement uncertainties, more than 99% of the initial model instances are falsified. The candidate model set obtained is the intersection of subsets of candidate models obtained for each of the 34 measurements. Note that measurements #LVDT, #33 and #45 are considered as outliers and are not used during model falsification. Table 1 and Figure 3 present the parameter values that compose the candidate model set. As shown in Figure 3, a single value

for both the rotational stiffness and the drift of the northern support are identified. This is due to the higher number of strain measurements in the northern side of the beam than in the southern side. Thus, more information is provided to reduce uncertainty on parameter values. On the southern support, despite a small reduction in the range of parameter values for the Young's modulus of steel and for the rotational stiffness of connections, the reduction in the number of combinations of these parameters is important.

Population-based prognosis

Using the 107 candidate models, the number of cycles to failure is computed using Equation 6 for a Category 90 detail ($m = 5$ and $C = 1.18 \times 10^{16}$ (Zhao et al. 2002)). Nominal stress ranges $\Delta \mathrm{g}_j(\boldsymbol{\theta}^*)$ are calculated at the weld toe position for each candidate model. For this case study, $\Delta\epsilon_{model,j}$ is based only on the model-simplification uncertainty because the profile dimension variability is already taken into account in S_n-N_f curves. The number of cycles to failure observed during the fatigue load test is compared with (1) the 95% confidence interval of the PDF for each prediction location obtained using the population-based prognosis methodology; and (2) the remaining-life prediction obtained using the design model. The design model is based on conservative assumptions such as pinned truss connections and the a-priori symmetrical static system with 0-values for the support rotational stiffness and the support drift, as well as a value of 210 GPa for the Young's modulus of steel. Figure 5 compares the number of cycles to failure obtained during this test with the values predicted using the candidate models, as well as using the design-model predictions. A range of 14 fatigue-failure observations is shown for comparison (Acevedo and Nussbaumer 2012) . The comparison of results shows that the remaining-fatigue-life predictions of the design model are more pessimistic than the candidate-model-prediction interval for each critical connection. This figure shows that the number of cycles observed through fatigue testing are much higher (more than 10 times) than candidate-model predictions for each connection. This is due to the high level of conservatism included in the S_n-N_f curves. Although the code specifications (Zhao et al. 2002) are limited to low profile thicknesses, detail Category 90 (Zhao et al. 2002) is suitable for this type of K-joint.

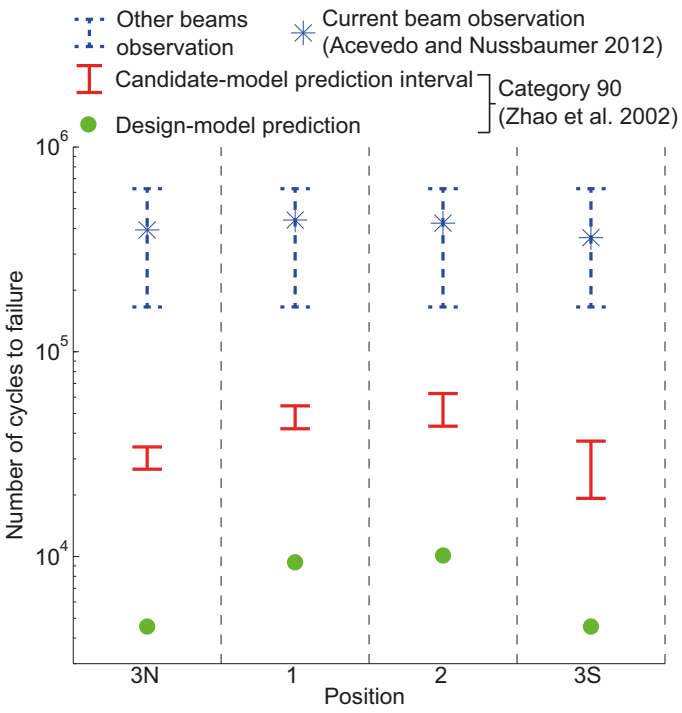

Figure 5. Comparison of the number of cycles to failure between fatigue-load tests (Acevedo and Nussbaumer 2012), design-model predictions and candidate-model-set predictions using detail Category 90 (Zhao et al. 2002)

The lowest candidate-model prediction is obtained for connection #3S (19 252 cycles), which is in agreement with the observation made during the fatigue-load test. Indeed, as presented in Table 3, the lowest observed number of cycles is 360 580 for connection #3S. This means that the prognosis methodology is capable of locating the weakest connection. Due the assumption of symmetrical boundary conditions, the design model fails to identify the weakest connection. Instead, it locates connections #3N and #3S as failing at the same time. As expected in the previous section, the prediction uncertainty at northern connections (#3N and #1) are lower than at the southern connections (#2 and #3S) due to the high number of measurements in that region. In Table 3, the comparison of the lower bound of the candidate-model-set predictions shows an improvement of the remaining fatigue life up to 487% for connection #3N.

The information provided by measurements, combined with the model-falsification methodology, results in better remaining-fatigue-life predictions while remaining conservative with respect

R. Pasquier, J.-A. Goulet, C. Acevedo and I. F.C. Smith, (2014).
Improving Fatigue Evaluations of Structures Using In-service Behavior Measurement Data.
Journal of Bridge Engineering, 19(11), 04014045. doi:10.1061/(ASCE)BE.1943-5592.0000619

Table 3. Remaining-fatigue-life prediction improvement for each critical connection as well as number of cycles observed during fatigue load test for the truss beam

Connection #	3N	1	2	3S
Observed number of cycle during fatigue test	393 360	439 550	424 650	360 580
CMS-prediction lower bound	26 699	42 037	43 269	19 252
Design-model prediction	4 545	9 378	10 125	4 545
Prediction improvement [%]	**487**	**348**	**327**	**324**

to experimental results. Thus, in this case study, the population-based prognosis methodology improves the remaining-fatigue-life predictions compared with predictions that are based on conservative design assumptions.

Aarwangen Bridge

Structure description

In this example, a composite steel-concrete bridge, located in the city Aarwangen (Switzerland) is studied. The bridge is made of welded tubular steel trusses acting in a composite manner with the concrete deck. Figure 6 shows the cross-section of the finite-element model of the structure and its general overview. The goal of this study is to provide better estimates of the reserve fatigue capacity of tubular welded connections. Several characteristics of the structure are unknown,

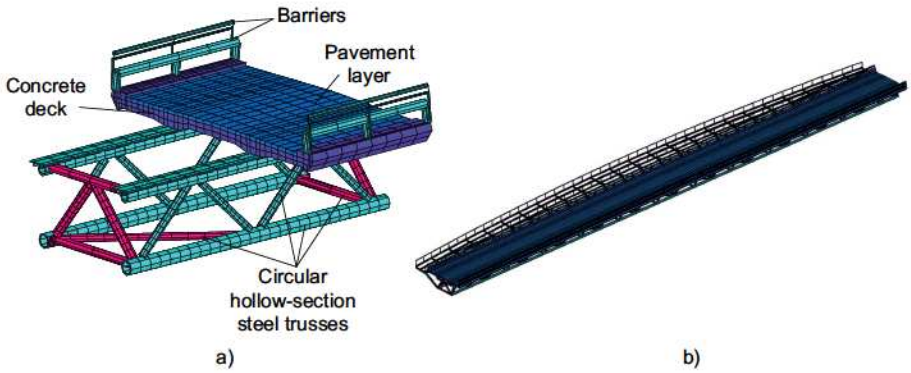

Figure 6. (a) Aarwangen Bridge model cross-section and (b) general overview

such as, the rotational stiffness of the truss connections, the longitudinal stiffness of the pavement covering expansion joints and the Young's moduli of steel, concrete and pavement. The stiffness

R. Pasquier, J.-A. Goulet, C. Acevedo and I. F.C. Smith, (2014).
Improving Fatigue Evaluations of Structures Using In-service Behavior Measurement Data.
Journal of Bridge Engineering, 19(11), 04014045. doi:10.1061/(ASCE)BE.1943-5592.0000619

parameters are modeled with rotational and longitudinal springs as illustrated in Figure 7. The

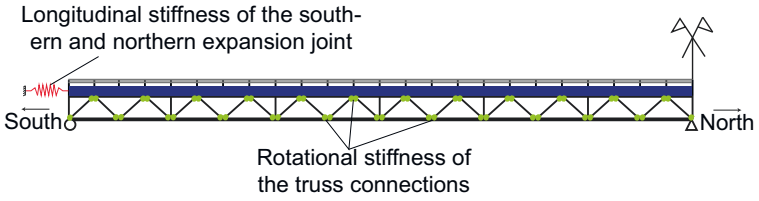

Figure 7. Model parameters to identify

rotational stiffness of the truss connections is represented by rotational springs connected between the diagonal members and either the upper or lower chord. Expansion joints are modeled using springs parallel to the bridge longitudinal axis. Possible parameter values for spring stiffnesses are sought for both the southern and northern abutments. These structural properties are to be identified using behavior measurements. Other uncertainties, such as concrete Poisson's ratio, truck weight and member dimensions, have a secondary influence on the structural behavior.

Measurements and load-test description

The static load test is performed using two trucks positioned according to three different configurations. The deformations were monitored using 18 strain gauges placed on truss members at different locations (see Figure 8 and Schumacher and Blanc 1999). Figure 9 shows the three truck

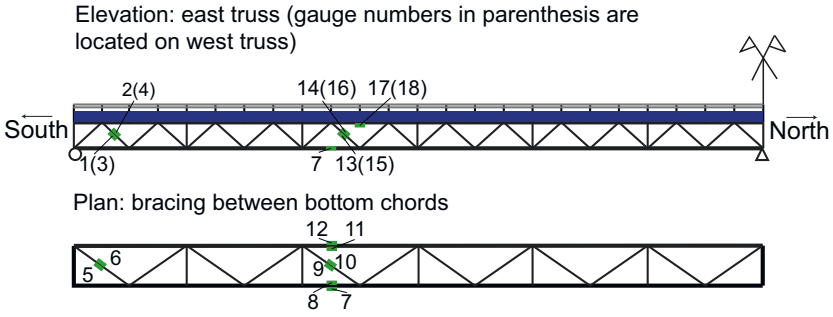

Figure 8. Strain-gauge locations (adapted from Schumacher and Blanc 1999)

configurations on the southern span of the bridge. For the first load case, a truck is centered on the east lane. In the second load case, a truck is centered on the west lane and in the third load case,

both trucks are positioned side by side.

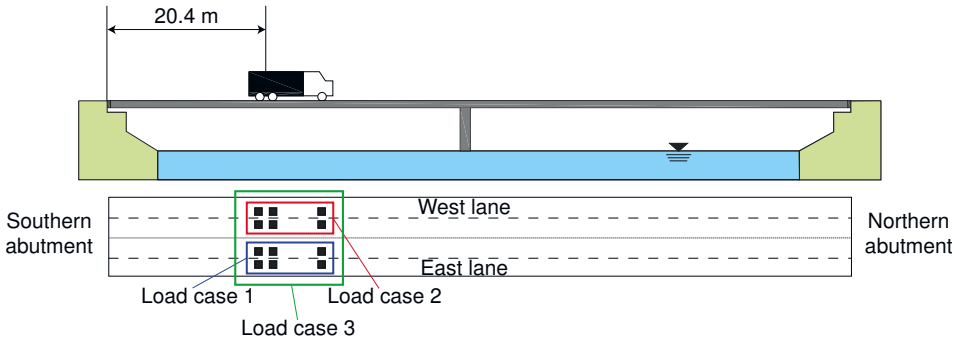

Figure 9. Static test load-case configurations (adapted from Schumacher and Blanc 1999)

Data interpretation

The data obtained from the three static-load tests are used to identify the values of unknown parameters. The initial model set is generated using values of the six parameters described in the previous section. Parameters $\boldsymbol{\theta} = [\theta_1, \theta_2, \ldots, \theta_6]$ and their initial range of values are presented in Table 4. The range of values for the spring stiffnesses have been determined by a sensitivity analysis. The ranges for the Young's moduli are estimated using engineering heuristics. Parameter ranges are divided into five values and combinations of parameter values are used to build an initial model set containing $15\,625$ instances. Figure 10 illustrates the combination of parameter values for a single model instance. Each axis represents the values of a parameter. After falsification, the falsified parameter values are displayed as full dots, while the candidate parameter values are represented as squares.

The values for model and measurement uncertainties ($U_{model,i}$ and $U_{measure,i}$) are computed by combining the uncertainty sources presented in Table 5. Uncertainties, such as concrete Poisson's ratio, truck weight, pavement thickness and profile dimensions are estimated through the evaluation of model-prediction variance using Monte Carlo sampling. Profile dimension variabilities are related to their design dimensions. The other PDFs are determined using field data and engineering heuristics. Additional uncertainties are conservative estimates for all other phenomena that

R. Pasquier, J.-A. Goulet, C. Acevedo and I. F.C. Smith, (2014).
Improving Fatigue Evaluations of Structures Using In-service Behavior Measurement Data.
Journal of Bridge Engineering, 19(11), 04014045. doi:10.1061/(ASCE)BE.1943-5592.0000619

Table 4. Initial-model parameter ranges and identified ranges for Aarwangen Bridge

Parameter θ	Units	Initial range	Identified range
Rotational stiffness of truss connections	MNm/rad	10^{-1}-10^{3}	10^{-1}-10
Stiffness of southern expansion joint	MN/m	10^{-1}-10^{4}	10^{-1}-10
Stiffness of northern expansion joint	MN/m	10^{-1}-10^{4}	10^{-1}-10
Young's modulus of steel	GPa	200-212	200-212
Young's modulus of concrete	GPa	20-50	27.5-50
Young's modulus of pavement	GPa	2-20	2-11

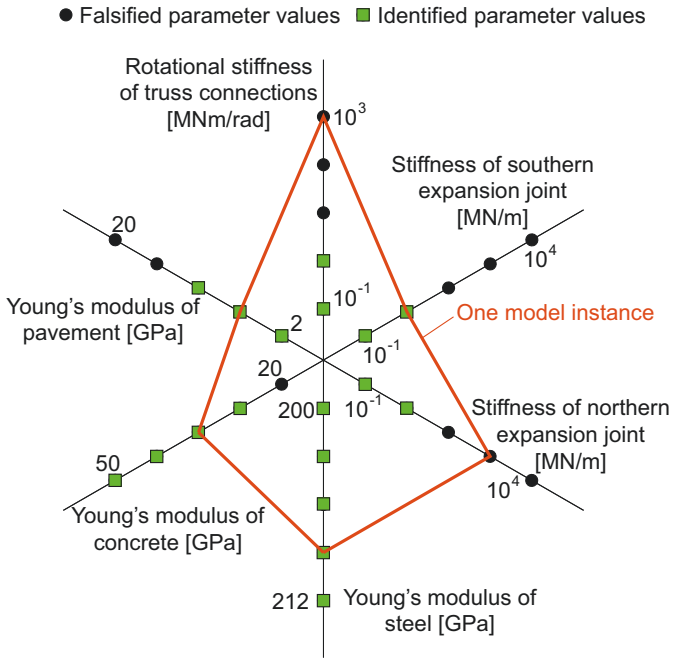

Figure 10. Single initial-model-instance generation from primary-parameter samples with falsified and identified parameter values for Aarwangen Bridge

individually have a negligible influence. Repeatability, truck position, model simplifications and FEM, mesh refinement and additional uncertainty are calculated with respect to the mean of initial-model-set prediction values. This table shows a histogram describing the relative importance of each uncertainty source for sensor location #13. The uncertainty in sensor resolution contributes the most to the total uncertainty. The model uncertainty, which is composed of all sources except sensor resolution, repeatability and cable losses, is responsible for 54.4% of the total uncertainty.

For a target probability $\phi = 0.95$, using seven strain measurements (#1, 2, 3, 13, 15, 17, 18) and

R. Pasquier, J.-A. Goulet, C. Acevedo and I. F.C. Smith, (2014).
Improving Fatigue Evaluations of Structures Using In-service Behavior Measurement Data.
Journal of Bridge Engineering, 19(11), 04014045. doi:10.1061/(ASCE)BE.1943-5592.0000619

Table 5. Aarwangen Bridge uncertainty sources and their probability density function as well as their relative importance with respect to the total uncertainty for sensor location #13

Uncertainty source	Unit	PDF	Mean/Min	STD/Max	Relative importance
Sensor resolution	$\mu\epsilon$	Uniform	-2	2	27%
Δt_2 steel profile thickness	%	Uniform	-12.5	12.5	19%
Repeatability	%	Gaussian	0	1.5	15%
Truck position	%	Uniform	-3	3	7.8%
ΔW truck-axle weight	kN	Uniform	-1	1	7.6%
Model simplifications and FEM	%	Uniform	0	5	6.7%
Cable losses	%	Uniform	-1.3	1.3	3.6%
Δt pavement thickness	%	Gaussian	0	2.5	3.1%
Mesh refinement	%	Uniform	-2	0	2.8%
Additional uncertainty	%	Uniform	-1	1	2.6%
ΔD_2 steel profile diameter	%	Uniform	-1	1	2.5%
Δt_1 steel profile thickness	%	Uniform	-10	10	1.4%
Δv Poisson's ratio of concrete	-	Gaussian	0.19	0.025	0.5%
ΔD_1 steel profile diameter	%	Uniform	-1	1	0.4%

three load cases, $15\,556$ model instances are falsified leading to a population of 69 candidate models. These seven measurements are at locations that are the most sensitive to changes in parameter values. Using measurements at locations that are not sensitive to the parameters is inefficient in the falsification process. In addition, use of the model falsification approach implies that outliers have been removed. In order to ensure the robustness of diagnosis, it is verified that a single measurement is not responsible for discarding more than 90% of the initial model instances. Among the 11 strain gauges that are not used, four are not functioning properly (#9, 10, 12, 14) as reported in Schumacher and Blanc (1999) and seven are redundant measurements (#4, 5, 6, 7, 8, 11, 16). These redundant measurements are not sensitive to changes in the parameter values. However, they confirm compatibility of the candidate models with the observation. Figure 11 presents the initial-model-set predictions for strain measurement #13 under load case 1 (see Figure 8). The continuous line represents the measured value and the dashed lines represent threshold bounds that are defined based on the combined uncertainty PDF. Each dot refers to the prediction of a model instance and stars are predictions of the identified candidate models. Model instances that are included in the threshold bounds which are not candidate models are model instances which have been rejected by

other measurements.

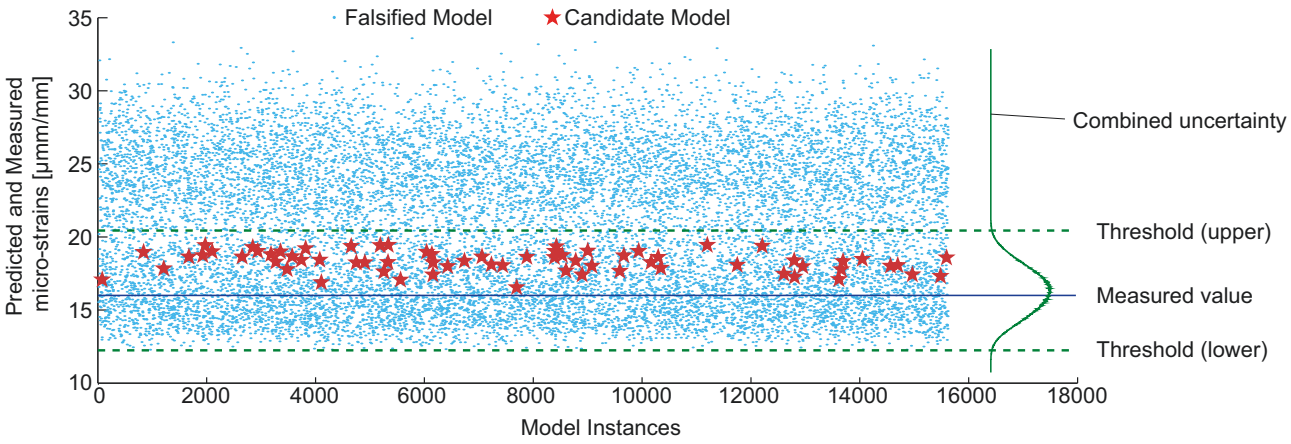

Figure 11. Candidate-model plot for strain measurement location #13 under load case 1

Table 4 and Figure 10 present the identified parameter values that compose the candidate model set. The results show that truss-connection and expansion-joint stiffnesses take low parameter values and the range of possible values is significantly reduced. The material Young's moduli, however, have only slightly decreased. Even for the Young's modulus of steel, the range of values remains the same as the initial range. This means that more measurements are required in order to reduce the uncertainty of these material properties. Despite this, the number of candidate models is greatly reduced compared to the number of initial model instances.

In-service behavior prognosis

The 69 candidate models identified using in-situ measurements are used to predict stresses as described in the population-based prognosis methodology. Two axle loads of 270 kN are applied on the west lane of the bridge finite-element model (SIA261 Code 2003). The influence lines of stresses are calculated for two truss connections. Each truss connection is composed of two welded diagonal members. Then, the study focuses on four critical construction details as shown in Figure 12. The maximum and minimum stresses are then computed from the influence lines. The maximum stress ranges $\Delta\sigma_j$ are determined based on Equation 4. The stress-range calculation takes into account a reduction to 60% of the compressive stresses in order to take advantage of

R. Pasquier, J.-A. Goulet, C. Acevedo and I. F.C. Smith, (2014).
Improving Fatigue Evaluations of Structures Using In-service Behavior Measurement Data.
Journal of Bridge Engineering, 19(11), 04014045. doi:10.1061/(ASCE)BE.1943-5592.0000619

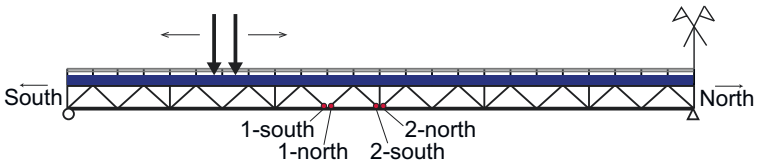

Figure 12. Critical truss connection locations and axle loading

the favorable effect of compressive stresses in the fatigue assessment (SIA263 Code 2003). In addition, the stress-ranges are multiplied by a damage equivalence factor $\lambda = 1.82$ and resistance factor $\gamma_{Mf} = 1$ (SIA263 Code 2003). The number of cycles to failure is then calculated using Equation 5 with $m = 5$ and $C = 1.18 \times 10^{16}$ for detail Category 90 (Zhao et al. 2002). The model uncertainty $\Delta\epsilon_{model,j}$ is combined with the same sources used with the data interpretation, except for the uncertainty of the steel profile thickness and diameter which are already included in the S_n-N_f curves. For this type of road, $500\,000$ heavy vehicles per year are assumed (SIA261 Code 2003) in order to determine the number of years to failure.

The PDFs of the number of years to failure obtained using the population-based approach are represented in Figure 13 for the initial model set (IMS) (without data interpretation) and for the candidate model set (CMS) (with data interpretation) for each critical connection. The combination of each parameter effect reveals a bimodal distribution of the model predictions. This shape is dependent on the choice of parameters to identify. Figure 13 also compares the distributions of the number of years to failure with the design-model predictions. The design model is composed of pinned truss connections without expansion joints or pavement, as well as design values for the Young's moduli of steel ($210\,$GPa) and concrete ($35\,$GPa).

The comparison of IMS-predictions with CMS-predictions reveals a great improvement of accuracy for the remaining fatigue life. The relative reduction with respect to their standard deviations is up to 90% for connection #2-north (see Table 6). Because the uncertainty is higher for the northern connections than for the southern connections, the reductions are the greatest. The information provided by measurements leads to falsifying more models describing the behavior of the northern connections than those for the southern locations. However, this is not necessarily the

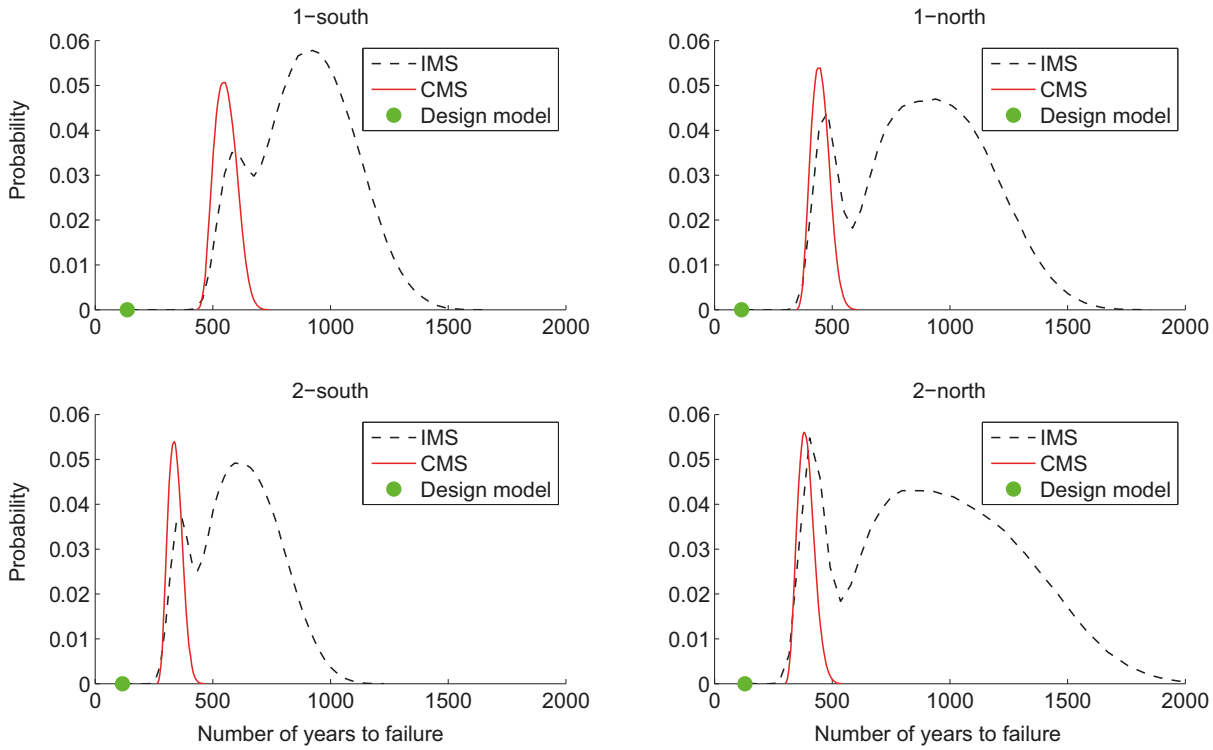

Figure 13. Comparison of number-of-years-to-failure predictions between the initial model set (IMS) and the candidate model set (CMS), as well as predictions made using a design model for connections 1-south, 1-north, 2-south and 2-north (see Figure 12)

case for the southern connections, for which the highest uncertainty is at connection #1-south, and the highest reduction is at connection #2-south. The response variability at a particular location depends on the sensitivity of the parameter values in the specific loading configuration. It is thus difficult to predict the response variability at a given location without analyzing the sensitivity of the parameters to the response.

Table 6 presents the CMS-prediction lower bound values corresponding to conservative values for the remaining-fatigue-life predictions. Lower bounds for prediction values are calculated by determining the shortest confidence interval that includes a probability content of 95% for each prediction location. In this study, the remaining fatigue life of these four connections is 289 years for a failure happening at connection #2-south. For the design-model prediction, the remaining fatigue life of these four connections would be 114 years for a failure at connection #1-north (see

Table 6). Compared with the predictions based on the population-based prognosis methodology, this leads to a prediction improvement of 235%. For connection #1-south, the improvement is up to 248%.

Table 6. Relative reduction between the IMS-predictions and the CMS-predictions with respect to the standard deviation and remaining-fatigue-life prediction improvement between the CMS-predictions and the design-model predictions

Connection #	1-south	1-north	2-south	2-north
Relative reduction [%]	**77**	**86**	**83**	**90**
CMS-predictions lower bound [years]	473	382	289	327
Design-model predictions [years]	136	114	116	128
Prediction improvement [%]	**248**	**235**	**149**	**155**

Through taking advantage of the data-interpretation techniques described in this paper, the reduction in predicted remaining fatigue life from the initial population (prior to having measurements) to candidate population of models is between 77% and 90% depending on the connection. In addition, data interpretation combined with an advanced modeling improves the remaining-fatigue-life predictions of the Aarwangen Bridge between 149% and 248%. Thus, measurement data provides useful information to enhance the accuracy of remaining-life predictions and to obtain less conservative prognostics than when using design models.

DISCUSSION

Remaining-fatigue-life predictions are sensitive to modeling uncertainties. Without using any measurements to reduce the uncertainty, the prediction distribution of the remaining fatigue life varies from 121 years to more than 1000 years for connection #2-north of the Aarwangen Bridge. When data are used to improve behavior models, the prediction distribution ranges from 298 years to 548 years. In practice, conservative and simplified models are often employed prior to more sophisticated evaluations. When expensive intervention is unavoidable, methodologies such as population-based prognosis help to more accurately evaluate existing structures. Indeed, the case study on the Aarwangen Bridge shows that measurement data are able to reduce the prognosis uncertainty while providing less conservative estimates of the remaining-life predictions than current

practice. This has the potential to lead to better evaluation of existing bridges, and as a result, more efficient maintenance and ultimately, replacement avoidance.

As shown in the truss-beam example, the population-based prognosis methodology is able to identify the weakest connection under fatigue loading. Given that structures can be measured adequately, population-based prognosis is able to evaluate the global safety of a structure by assessing any critical detail without being limited to the locations where measurements are available.

Although the S_n-N_f curves are conservative as shown in the truss-beam example, improvement of remaining-fatigue-life prediction would be possible if a more accurate fatigue-damage model is employed. In addition, the traffic-load model is also conservative. This means that more sophisticated fatigue-damage and traffic-load models, coupled with the population-based prognosis methodology, would further decrease the conservatism in the remaining-fatigue-life predictions.

CONCLUSION

The population-based prognosis methodology takes advantage of information obtained from measurement data to improve the accuracy of remaining-fatigue-life predictions. A first experimental investigation confirms that compared with traditional engineering approaches, the methodology provides less conservative estimations of remaining fatigue life. A second application on a full-scale bridge also confirms that using load-test data reduces the uncertainty associated with remaining-fatigue-life predictions.

ACKNOWLEDGEMENTS

The authors acknowledge ICOM (Steel Structures Laboratory), EPFL for providing test results (Acevedo and Nussbaumer 2012; Acevedo et al. 2011), bridge drawings and monitoring data and Yves Reuland for the work done on the truss-beam example. This work was partially funded by the Swiss national Science Foundation under contract no. 200020-144304.

References

AASHTO (2007). *LRFD Bridge Design Specifications, 4th Edition*. American Association of State Highway and Transportation Officials, Washington, DC.

Acevedo, C. and Nussbaumer, A. (2012). "Effect of tensile residual stresses on fatigue crack growth and S-N curves in tubular joints loaded in compression." *International Journal of Fatigue*, 36(1), 171–180.

Acevedo, C., Nussbaumer, A., and Drezet, J. M. (2011). "Evaluation of residual welding stresses and fatigue crack behavior in tubular K-joints in compression." *Stahlbau*, 80(7), 483–491.

ASME (2006). *Guide for verification and validation in computational solid mechanics*. ASME.

Beven, K. J. (2006). "A manifesto for the equifinality thesis." *Journal of Hydrology*, 320(1-2), 18–36.

Beven, K. J., Smith, P. J., and Freer, J. E. (2008). "So just why would a modeller choose to be incoherent?." *Journal of hydrology*, 354(1-4), 15–32.

Chan, T. H. T., Li, Z. X., and Ko, J. M. (2001). "Fatigue analysis and life prediction of bridges with structural health monitoring data – Part ii: application." *International Journal of Fatigue*, 23(1), 55–64.

Cheung, S. H. and Beck, J. L. (2009). "Bayesian model updating using hybrid Monte Carlo simulation with application to structural dynamic models with many uncertain parameters." *Journal of Engineering Mechanics*, 135(4), 243–255.

EN1993-1-9 (2005). *Eurocode 3 - Design of steel structrures - Part 1-9: Fatigue*. European committee for standardization.

Fisher, J. W., Kulak, G. L., and Smith, I. F. C. (1998). *A fatigue primer for structural engineers*. National Steel Bridge Alliance.

Goulet, J.-A., Michel, C., and Smith, I. F. C. (2012). "Hybrid probabilities and error-domain structural identification using ambient vibration monitoring." *Mechanical Systems and Signal Processing*, 37(1-2), 199–212.

Goulet, J.-A. and Smith, I. F. (2013a). "Structural identification with systematic errors and unknown uncertainty dependencies." *Computers & Structures*, 128, 251–258.

Goulet, J.-A. and Smith, I. F. C. (2013b). "Predicting the usefulness of monitoring for identifying the behaviour of structures." *Journal of Structural Engineering*, in press.

Guo, T. and Chen, Y.-W. (2013). "Fatigue reliability analysis of steel bridge details based on field-monitored data and linear elastic fracture mechanics." *Structure and Infrastructure Engineering*, 9(5), 496–505.

Guo, T., Frangopol, D. M., and Chen, Y.-W. (2012). "Fatigue reliability assessment of steel bridge details integrating weigh-in-motion data and probabilistic finite element analysis." *Computers & Structures*, 112, 245–257.

Hobbacher, A. (2012). "Recommendations for fatigue design of welded joints and components." *Report No. XIII-1965-03*, IIW/IIS.

JCGM (2011). *Evaluation of measurement data – Supplement 2 to the "Guide to the expression of uncertainty in measurement" – Extension to any number of output quantities*, Vol. JCGM 102:2011. JCGM Working Group of the Expression of Uncertainty in Measurement.

Liu, M., Frangopol, D. M., and Kwon, K. (2010). "Fatigue reliability assessment of retrofitted steel bridges integrating monitored data." *Structural Safety*, 32(1), 77–89.

MacKay, D. (2003). *Information theory, inference, and learning algorithms*. Cambridge Univ Press.

Orcesi, A. D. and Frangopol, D. M. (2010). "Inclusion of crawl tests and long-term health monitoring in bridge serviceability analysis." *Journal of Bridge Engineering*, 15(3), 312–326.

Papadimitriou, C., Fritzen, C.-P., Kraemer, P., and Ntotsios, E. (2011). "Fatigue predictions in entire body of metallic structures from a limited number of vibration sensors using Kalman filtering." *Structural Control and Health Monitoring*, 18(5), 554–573.

Schumacher, A. and Blanc, A. (1999). "Stress measurements and fatigue analysis on the new bridge at Aarwangen." *Report No. 386*, ICOM, EPFL, Switzerland.

SIA261 Code (2003). *Norme SIA 261: Actions on Structures*. SIA Zurich.

SIA263 Code (2003). *Norme SIA 263 : Steel structures*. SIA Zurich.

Šidák, Z. (1967). "Rectangular confidence regions for the means of multivariate normal distributions." *Journal of the American Statistical Association*, 62, 626–633.

Siriwardane, S., Ohga, M., Dissanayake, R., and Taniwaki, K. (2008). "Application of new damage

indicator-based sequential law for remaining fatigue life estimation of railway bridges." *Journal of Constructional Steel Research*, 64(2), 228–237.

Soliman, M., Frangopol, D. M., and Kown, K. (2013). "Fatigue assessment and service life prediction of existing steel bridges by integrating SHM into a probabilistic bi-linear S-N approach." *Journal of Structural Engineering*, in press.

Strauss, A., Frangopol, D. M., and Kim, S. (2008). "Use of monitoring extreme data for the performance prediction of structures: Bayesian updating." *Engineering Structures*, 30(12), 3654–3666.

Sweeney, R. A. P. (1976). "The load spectrum for the fraser river bridge at New Westminster, BC." *Presented at the 75th Technical Conference, AREA, Chicago, Illinois, 22-24 March 1976.*, Vol. 77.

SZS (2005). *Konstruktionstabellen. C5/05 steel work*. Stahlbau Zentrum Schweiz.

Uzgider, E., Sanli, A. K., Piroglu, F., Ozgen, A., Caglayan, B. O., and Tektunali, A. C. (1996). "Testing & evaluation of Karacam railway Bridge." *Report No. 5*, NATO Science for Stability Programme TU-850-BRIDGES Research Project Report, Istanbul Technical University, Civil Engineering Faculty, Structural Departement, Istanbul, Turkey.

Ye, X. W., Ni, Y. Q., Wong, K. Y., and Ko, J. M. (2012). "Statistical analysis of stress spectra for fatigue life assessment of steel bridges with structural health monitoring data." *Engineering Structures*, 45(0), 166–176.

Yuen, K. V. (2010). *Bayesian methods for structural dynamics and civil engineering*. Wiley.

Zhang, E., Feissel, P., and Antoni, J. (2011). "A comprehensive Bayesian approach for model updating and quantification of modeling errors." *Probabilistic Engineering Mechanics*, 26(4), 550–560.

Zhao, X.-L., Herion, S., Packer, J. A., Puthli, R. S., Sedlacek, G., Wardenier, J., Weynand, K., van Wingerde, A. M., and Yeomans, N. F. (2002). *Design guide for circular and rectangular hollow section welded joints under fatigue loading*. TÜV-Verlag GmbH.

Zhou, Y. E. (2006). "Assessment of bridge remaining fatigue life through field strain measure-

ment." *Journal of Bridge Engineering*, 11(6), 737–744.